The 6th European sCO_2 Conference for Energy Systems
April 09-11, 2025, Delft, The Netherlands

2025-sCO2.eu-194

CHALLENGES IN SCALING sCO_2 COMPRESSOR SPEEDLINE TO DIFFERENT INTAKE THERMODYNAMIC CONDITIONS

Alessandro Romei*
Laboratory of Fluid Machines
Department of Energy, Politecnico di Milano
Via Raffaele Lambruschini 4a, Milano, Italy
Email: alessandro.romei@polimi.it

Giacomo Persico
Laboratory of Fluid Machines
Department of Energy, Politecnico di Milano
Via Raffaele Lambruschini 4a, Milano, Italy

ABSTRACT

Compressors operating with carbon dioxide near the critical point experience complex aerothermodynamic phenomena, where deviations from perfect-gas similarity and two-phase flow effects dominate. Existing models inadequately capture the impact of intake thermodynamic conditions on the choked flow rate, leaving a gap in predictive capabilities for these machines. This work addresses this gap by deriving a correlation to predict the choked flow rate as a function of two generalized parameters: the cavitation/condensation parameter and the isentropic pressure-volume coefficient, which describe two-phase and non-ideal effects.

A database of 100 speedlines, generated through CFD simulations with varying thermodynamic conditions and fixed peripheral Mach number, was used to train a symbolic regression algorithm based on gene expression programming. This method was chosen to derive an explicit, easy-to-use analytical expression without assuming a priori functional forms.

Results showed that the choked flow rate could vary from 90% to 155% of the nominal value depending on thermodynamic conditions, highlighting the dominant role of the two parameters. The derived correlation demonstrated trends consistent with CFD predictions, with an accuracy of ±3 percentage points for most cases. However, an *a-posteriori* validation against varying peripheral Mach numbers and an alternative impeller geometry revealed significant discrepancies, underscoring the interplay between thermodynamic conditions, geometry, and aerodynamics. This analysis showed that the peripheral Mach number and the geometric features influence choking behavior unpredictably, limiting the correlation's general applicability.

While the proposed correlation is not adequate for quantitative scaling across designs, it provides preliminary insights into qualitative trends. For accurate predictions, high-fidelity CFD remains necessary, highlighting the inherent challenges of universal scaling for near-critical operations in sCO_2 compressors.

INTRODUCTION

Having an early understanding of the performance map of a centrifugal compressor is crucial during the design process, especially when detailed data about the full compressor geometry is unavailable [1]. Most methods for estimating compressor performance maps rely on perfect-gas assumptions and extensively use similarity theory. However, for compressors operating with CO_2 near the critical point, these assumptions break down due to the severe non-ideality of the flow in this thermodynamic region [2]. Furthermore, once a design is finalized and performance maps are established for specific intake thermodynamic conditions, there is a lack of standardized methods to generalize these maps for other thermodynamic states.

Scaling methods that overcome the limitations of perfect-gas assumptions have been proposed for supercritical CO_2 (sCO_2) applications. For instance, Wright et al. [3], in their report on the Sandia compressor tests, scaled performance maps using critical quantities, following the pioneering work of Glassman [4]. However, experimental data exhibited notable scatter around the reference speedline. Baltadjiev [2] introduced a dimensionless flow rate formulation that accounts for non-ideal effects through compressibility and pressure-volume coefficients. While this approach captured non-ideal gas effects, it observed changes in choke margins of up to 9% with varying intake thermodynamic conditions. Similarly, Pham et al. [5] proposed scaling methods based on the pressure-volume isentropic coefficient, demonstrating their ability to predict changes in pressure ratio. However, none of these works accounted for two-phase flow effects, which are crucial near the critical point.

Two-phase effects are particularly relevant in megawatt-scale compressors near the critical point. Experimental campaigns by Toni et al. [6] revealed significant reductions in choked flow rates due to phase transitions, linked to abrupt drops in the speed of sound. This trend was corroborated by

* corresponding author

DOI: 10.17185/duepublico/83307

experimental data reported by Mortzheim et al. [7], though not explicitly discussed in their paper. Romei et al. [8] introduced a generalized cavitation/condensation parameter to interpret two-phase effects and their impact on choking, but they did not provide a scaling procedure. Similarly, Anderson [9] proposed a method incorporating isentropic expansion and velocity triangles to estimate choked flow rates, but this approach required additional geometry-specific variables and still failed to predict choking consistently under all tested conditions.

This work addresses the challenge of scaling compressor speedlines for variable thermodynamic intake conditions, focusing particularly on capturing the influence of non-ideal and two-phase flow effects on the choked flow rate. The goal is to derive an explicit, easy-to-use correlation that links the choked flow rate to thermodynamic states and operating conditions, providing a practical tool for compressor design.

The paper is structured as follows. First, the governing assumptions and parameterization of thermodynamic effects are introduced. The methodology, including CFD simulations and symbolic regression techniques, is described next. Results are then presented, examining the correlation's accuracy and limitations in capturing the effects of thermodynamic state, Mach number, and impeller geometry. Finally, the implications and recommendations for future work are discussed.

COMPUTATIONAL METHOD

The compressor performance is evaluated using a steady pressure-based flow solver specifically developed for sCO_2 compressors [10]. This solver accounts for two-phase flows and employs accurate equations of state. Thermo-physical properties are computed using pressure and specific enthalpy as state variables, under the assumption of thermodynamic equilibrium between phases. The equation of state [11] and transport property correlations [12, 13] are incorporated into the solver through look-up tables, with their resolution detailed in the original reference [10]. Numerical discretization methods, the computational domain, the grid convergence study, and boundary conditions are described in Romei et al. [14]. The solver has been validated against experimental data from a megawatt-scale sCO_2 compressor stage [15], accurately predicting the choking flow rate within 3% of the experimental value.

The flow range along the speedline (i.e., fixing the peripheral Mach number) is constrained between the surge and choking limits. The surge limit is determined by progressively reducing the mass flow rate at the outlet until the total-to-static pressure ratio begins to decrease [16]. The maximum value of the total-to-static pressure ratio is then identified using a bisection method with a mass flow rate tolerance of 1%. Conversely, the choking limit is established by specifying the outlet static pressure and gradually decreasing it until the mass flow rate change falls below 1%.

EFFECT OF VARIABLE INTAKE THERMODYNAMIC CONDITIONS ON COMPRESSOR SPEEDLINE

This section examines the expected deviations from perfect-gas similarity in centrifugal compressors operating with carbon dioxide near its thermodynamic critical point and introduces appropriate dimensionless parameters to account for these additional effects. For a family of geometrically similar compressors, perfect-gas similarity implies that any dimensionless performance parameters (e.g., efficiency, work coefficient, pressure ratio, etc.) are functions of:

- The flow coefficient, $\phi = \dot{m}/(\rho_0 u_2 D_2^2)$, as a measure of the dimensionless volumetric flow rate;
- The machine (or peripheral) Mach number, $M_u = u_2/c_0$, representing compressibility effects;
- The machine (or peripheral) Reynolds number, $Re_u = \rho_0 u_2 L/\mu_0$, where L is a characteristic length (e.g., outlet blade height or meridional blade length), accounting for viscous effects;
- The ratio of specific heats $\gamma = c_p/c_v$, characterizing the specific fluid thermodynamics.

While flow coefficient, Mach number, and Reynolds number remain meaningful regardless of the flow thermodynamics, the ratio of specific heats is a reliable descriptor of flow processes within turbomachinery only when the fluid thermodynamics can be approximated as a polytropic ideal gas. This limitation is well-documented in the literature, and alternative parameters have been proposed as more effective scaling descriptors [2, 17, 18]. Among the possible parameters, and in line with previous works on sCO_2 compressors [5, 8], the generalized (or pressure-volume) isentropic coefficient evaluated at the intake total state is employed to account for non-ideal gas thermodynamics due to its direct relationship with Eulerian work. It is defined as:

$$k = \frac{\rho}{P}\left(\frac{\partial P}{\partial \rho}\right)_s = \frac{\rho}{P}\, c^2 \tag{1}$$

In addition to non-ideal gas effects, the presence of two-phase flows can also influence the compressor speedline, as experimentally demonstrated by Toni [6]. Two-phase flows induce early choking due to the abrupt decrease in the speed of sound when the local thermodynamic state intersects the saturation curve. In a previous work [8], drawing inspiration from hydraulic machines, the authors proposed the following generalized cavitation (or condensation) parameter:

$$C = \frac{2\big(h_o - h_{sat}(s_0)\big)}{u_1^2} = \frac{2\big(h_0 - h_{sat}(s_0)\big)}{f^2\, M_u^2\, c_0^2} \tag{2}$$

The parameter compares the kinetic energy required to reach saturation, assuming an isentropic expansion, with the peripheral velocity at the intake region, serving as an estimate of the relative flow velocity. It can also be directly linked to the peripheral Mach number through the diameter ratio $f = D_1/D_2$, which typically ranges between 0.35 and 0.50.

DOI: 10.17185/duepublico/83307

To illustrate the impact of these two parameters on the compressor speedline ($M_u = 0.7$), four distinct thermodynamic conditions are selected to isolate the individual effects of k and $\mathcal{C}$. Reynolds number effects are neglected hereinafter, as the high Reynolds number (on the order of 10^8), as a consequence of the high density and low dynamic viscosity, ensures fully turbulent flows and, hence, Reynolds number self-similarity. The four cases are presented in the temperature - specific entropy diagram shown in Figure 1.

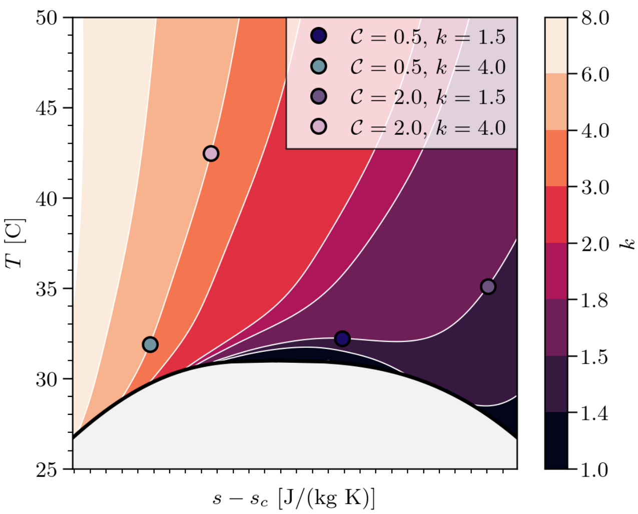

Figure 1: Intake thermodynamic conditions with different non-ideal gas effects and two-phase effects.

The reference compressor is a single-stage centrifugal compressor featuring a shrouded impeller and a vaneless diffuser. The main design parameters are $\phi_D = 0.04$, $\phi_2 = 0.20$, $M_u = 0.7$, and $\lambda_{eul} = 0.65$, following the design methodology proposed by Romei et al. [14]. The impeller includes 8 main blades and 8 splitter blades, selected on the basis of blade loading considerations.

The four speedlines corresponding to the different intake thermodynamic conditions are shown in Figure 2, expressed in terms of total-total isentropic efficiency, work coefficient (including parasitic losses), and total-total pressure ratio. Along the speedline, where the peripheral Mach number remains constant, Reynolds number effects are negligible, and the fluid is unchanged, the perfect-gas similarity would predict no variations in performance parameters. However, the results in Figure 2 contradict this expectation.

Specifically, the efficiency and work coefficient curves generally overlap until approaching the choked flow rate, which instead varies across the selected conditions. Notably, the choked flow rate changes significantly, from ϕ_C/ϕ_D = 105% to 154%. Minor differences are also observed in the computed surge flow rate (ϕ_S/ϕ_D), though these variations are limited to a few percent and are subject to higher uncertainty due to the steady-state assumptions of the flow solver.

Finally, beyond changes in the choked flow rate, the total-to-total pressure ratio curves also vary as a function of the isentropic coefficient. Intuitively, as the efficiency and work coefficient curves overlap, altering the fluid's compressibility from liquid-like ($k = 4.0$) to vapor-like ($k = 1.5$) results in different amounts of work being converted into pressure rise. Mathematically, this relationship can be approximated as:

$$\lambda \cdot \eta \approx \frac{1}{M_u^2} \frac{1}{k-1} \left(\Pi^{\frac{k-1}{k}} - 1 \right) \tag{3}$$

This relationship can be utilized for scaling purposes or simply to predict the corresponding variation in the pressure ratio when the intake total state, and consequently the fluid compressibility, changes.

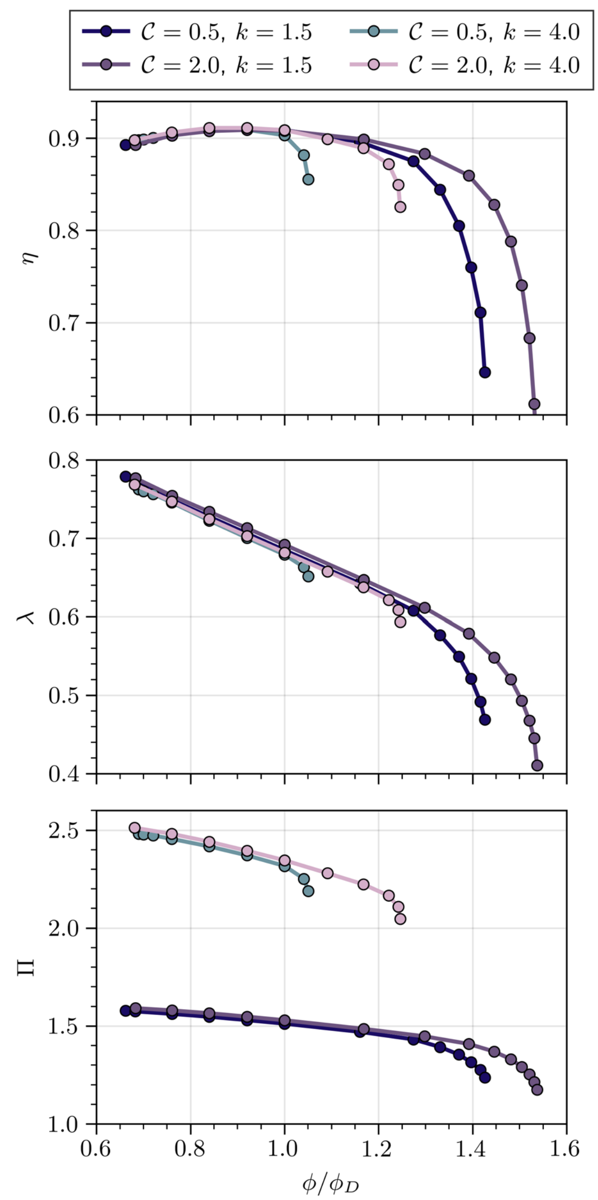

Figure 2: Speedline change with four distinct intake thermodynamic conditions.

DOI: 10.17185/duepublico/83307

To predict how a speedline changes with variations in the intake total state, the primary challenge lies in understanding the behavior of ϕ_C/ϕ_D . Both k and $\mathcal{C}$ significantly influence the choked flow rate, as evident in Figure 2. To better elucidate this relationship, the Mach number field and the mass fraction of the secondary phase are shown in Figure 3.

Consistent with the definition of $\mathcal{C}$, when $\mathcal{C} = 2.0$, the kinetic energy required to achieve saturation exceeds the flow kinetic energy, and consequently, no secondary phase is observed regardless of k. Conversely, when $\mathcal{C} = 0.5$, the flow kinetic energy exceeds the energy required for saturation, causing the formation of a secondary phase. Notably, while the two-phase region is comparable for $k = 1.5$ and $k = 4.0$, the amount of mass fraction is consistently higher for $k = 4.0$. This discrepancy arises from the fundamentally different properties of the secondary phase in the two cases.

When $k = 4.0$, the secondary phase is less dense and hence it tends to occupy a larger specific volume, leading to a significant reduction in the mixture density. This reduction facilitates greater acceleration of the mixture, increasing penetration into the saturation dome and consequently amplifying the amount of the secondary phase. In contrast, for $k = 1.5$, the secondary phase has a lower specific volume, causing minimal variation in the mixture density. As a result, the flow accelerates similarly to a single-phase flow, limiting its penetration into the two-phase dome.

The variation in mixture compressibility directly affects the speed of sound, and consequently, the Mach number. Specifically, the speed of sound drops sharply at the onset of the secondary phase, leading to a local increase in the Mach number and, as documented by Toni et al. [6], an early choking of the compressor. Figure 4 illustrates the reduction in the speed of sound along the saturation curve, parameterized by s/s_c. When the primary phase is liquid-like ($s/s_c < 1$), as in the case of $k = 4.0$, the drop in the speed of sound is significantly more pronounced compared to the vapor-like case ($s/s_c > 1$).

Based on these observations, the combination of $\mathcal{C}$ (which quantifies the compressor susceptibility to cavitation or condensation) and k (which reflects whether the secondary phase is lighter or denser) effectively explains the observed trends in ϕ_C/ϕ_D. As shown in Figure 3, the free-stream Mach number remains low (~0.3) despite the peripheral Mach number being 0.7. The onset of choking is primarily driven by the Mach number peak that occurs with the appearance of the secondary phase. Consequently, speedlines with $\mathcal{C} = 0.5$ exhibit earlier choking compared to cases with $\mathcal{C} = 2.0$, as a smaller increase in the flow rate is needed for the two-phase flows to occupy the throat section entirely. Among cases with the same $\mathcal{C}$, those with $k = 4.0$ choke earlier because the speed of sound in the two-phase mixture is significantly lower, causing the Mach number to reach unity more rapidly.

The objective of this paper is to generalize this behavior and develop a quantitative method to predict ϕ_C/ϕ_D when the intake total state changes. In general terms, the choked flow rate depends on the peripheral Mach number, the compressor geometry in the throat region, and the two parameters introduced to account for non-ideal and two-phase effects. Analytically:

$$\frac{\phi_C}{\phi_D} = \text{function}\ (M_u, k, \mathcal{C}, \text{shape}) \tag{4}$$

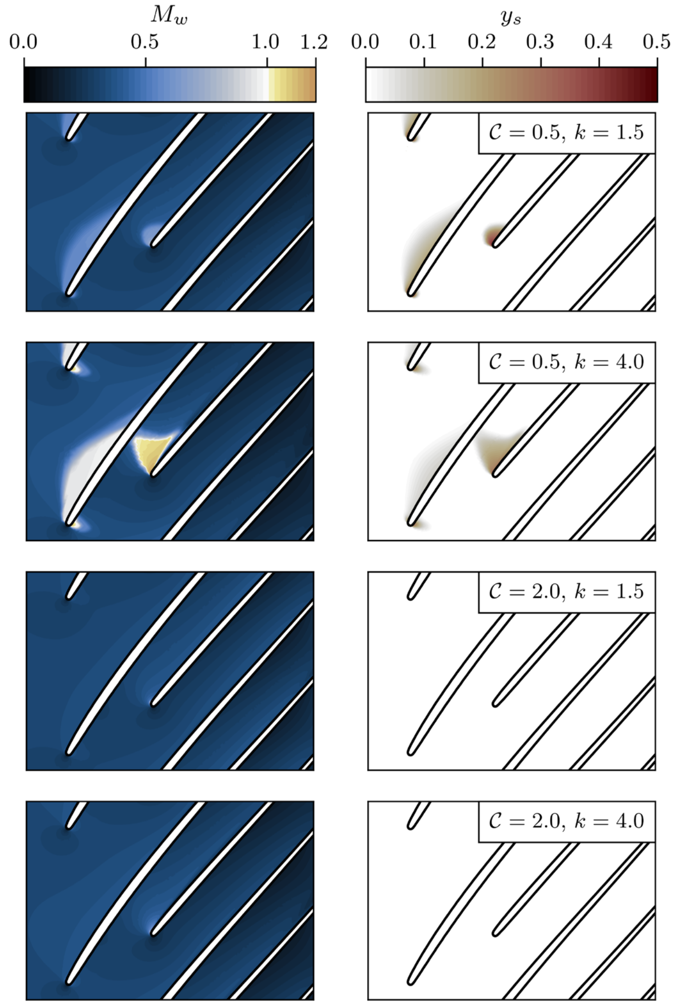

Figure 3: Fields at midspan of Mach numbers and mass fraction of the secondary phase for different intake total states.

Based on the previous observations, choking appears to be more closely associated with the onset of the secondary phase than with the free-stream Mach number in the single-phase region. Consequently, as a simplified assumption, the explicit dependence on the peripheral Mach number is omitted, resulting in the following mathematical relationship:

$$\frac{\phi_C}{\phi_D} = \text{function}\ (k, \mathcal{C}, \text{shape}) \tag{5}$$

DOI: 10.17185/duepublico/83307

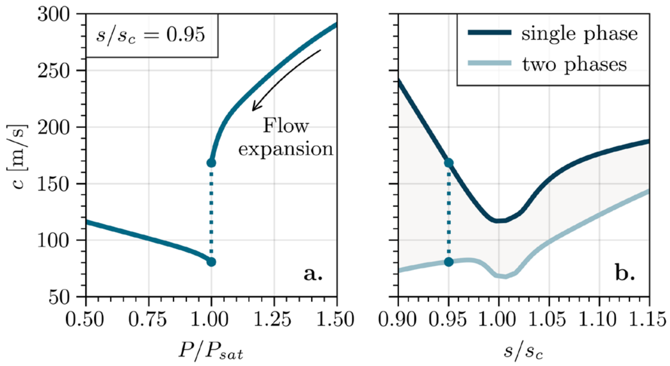

Figure 4: Evolution of the speed of sound along an isentrope (a) and drop in the speed of sound along the saturation curve (b).

It is important to note that the peripheral Mach number remains implicitly included in the definition of the $\mathcal{C}$ parameter. For a given thermodynamic state, $\mathcal{C}$ is inversely proportional to the peripheral Mach number. As such, a higher peripheral Mach number corresponds to a smaller $\mathcal{C}$, facilitating the onset of the secondary phase and leading to earlier choking.

Finally, it is assumed that, despite its overall significance, most impellers designed for sCO_2 applications exhibit a similar front loading, minimizing the likelihood of secondary phase onset. Naturally, a larger throat area could delay choking to higher flow rates, likely at the expense of a reduced surge margin. However, this study focuses on a single compressor representative of a family of compressors that follow the design approach proposed by Romei et al. [14]. As an additional simplified assumption, the dependence on the specific shape of the impeller throat region is also omitted, further simplifying the relationship to:

$$\frac{\phi_C}{\phi_D} = \text{function}\ (k, \mathcal{C}) \tag{6}$$

DESIGN OF EXPERIMENTS

To derive the functional expression in Equation (6), a design of experiments was generated comprising 80 distinct thermodynamic conditions, sampled using Latin Hypercube Sampling within the ranges $1.4 < k < 8.0$ and $0.2 < \mathcal{C} < 2.0$. These conditions fall within the thermodynamic region where the computational model, based on the homogeneous equilibrium model, has been demonstrated by Toni et al. [6] to predict the choked flow rate with a maximum error of 3%. The sampled thermodynamic states are plotted in the temperature-specific entropy diagram in Figure 5.

In the vapor-like region near the critical point ($s/s_c > 1$), the sampling technique fails to generate any points. This is due to the non-monotonic behavior of the isentropic coefficient k in this region, as highlighted by the isolines at $k = 1.4$. Multiple thermodynamic states, in terms of pressure and temperature, correspond to the same combinations of k and $\mathcal{C}$. Among the various admissible solutions, only those where the k-isolines exhibit monotonic behavior are selected for analysis.

These selected states are used to train a regression model, which is subsequently tested on 20 additional thermodynamic conditions scattered throughout the same region and generated using the same sampling logic. The same compressor geometry as described in the previous section is employed as a reference, with the peripheral Mach number held constant at 0.70. For each thermodynamic state, the choked flow rate is determined via sequential CFD calculations, progressively reducing the outlet static pressure until the mass flow rate variation between sequential runs falls below 1%.

The resulting curves are presented in Figure 6, illustrating a continuous variation of ϕ_C/ϕ_D ranging from values below unity to as high as 1.55, solely due to changes in the intake thermodynamic state. Among the 100 total curves (training and testing data), two (one from the training set and one from the testing set) exhibit a choking limit below the nominal flow rate. These cases correspond to conditions where k is high (indicating liquid-like properties and a significant drop in the two-phase speed of sound) and $\mathcal{C}$ is small, reflecting a high fraction of two-phase flow. Additionally, three curves (two training and one testing) choke near the nominal flow rate.

This wide variation in ϕ_C/ϕ_D underscores the critical influence of the thermodynamic state on determining the choked flow rate.

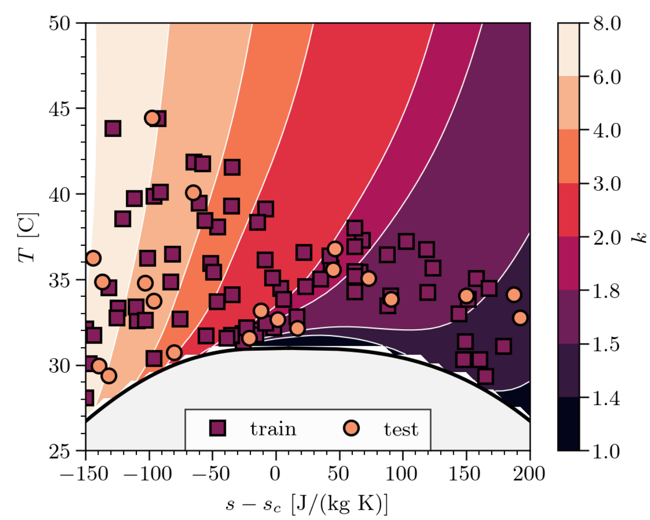

Figure 5: Sampled thermodynamic conditions for training and testing a regression model to predict the choked flow rate.

GENE EXPRESSION PROGRAMMING

In selecting the most suitable regression model, an explicit formulation is preferred over more complex regression algorithms (e.g., Gaussian processes) to facilitate its integration into off-design system analyses. For this purpose, gene expression programming, as implemented in the *gplearn* Python package, is employed. This method performs symbolic

DOI: 10.17185/duepublico/83307

regression without imposing a predefined functional form. Instead, it optimizes the relationship by combining a set of mathematical operators (e.g., addition, subtraction, multiplication, square root, etc.) using an evolutionary optimization algorithm.

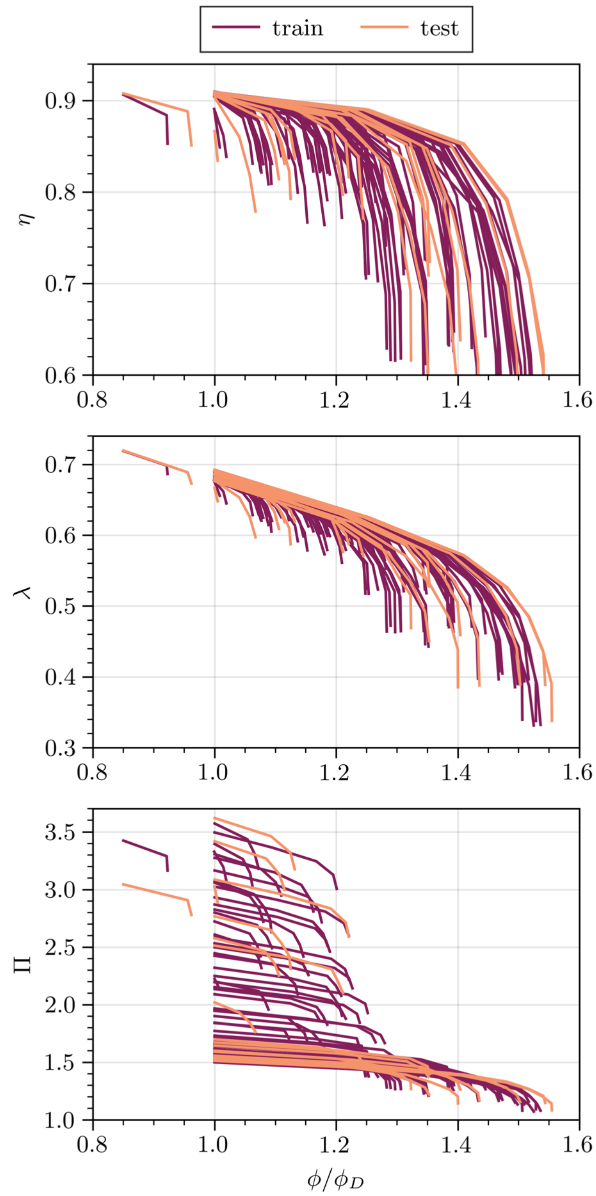

Figure 6: Speedlines for training and testing data

The objective function for the optimization is the minimization of the root mean square error (RMSE) between the training data and the fitted relationship. A low parsimony coefficient of 0.01 is chosen to allow for more complex functional relationships if they can improve the model's accuracy. To ensure robustness, 20 parallel optimizations are performed with different random seed initializations, and the relationship with the lowest RMSE among the trials is selected. The optimization yields the following explicit function, achieving an R^2 value of 0.98:

$$\frac{\widehat{\phi_C}}{\phi_D} - 1 = \frac{1}{\sqrt{k(k^2 + \mathcal{C})}(k - 0.285)} + 0.110\,\mathcal{C} \tag{7}$$

The derived expression highlights the interplay between k and $\mathcal{C}$, demonstrating that their contributions to the determination of ϕ_C/ϕ_D are not independent. To assess its predictive capability, the expression is evaluated against the test dataset, comprising results independent of those used during optimization. The predictions are presented in the parity plot in Figure 7. Most data points fall within a ±3% band, consistent with the accuracy of the CFD predictions relative to experimental measurements.

Five data points lie outside this accuracy range, with errors as high as 10 percentage points. These correspond to cases where the choked flow rate is below the nominal value, a condition where the correlation was trained on only a single data point, leading to expected regression inaccuracies. Additionally, three test points show errors of approximately 6%, occurring in conditions where choking is predicted near the nominal flow rate.

From a technical perspective, these deviations are not critical. When the correlation predicts $\frac{\widehat{\phi_C}}{\phi_D} - 1 < 10\%$, the margin to choking is small, suggesting that more detailed analyses are warranted to confirm the actual margin.

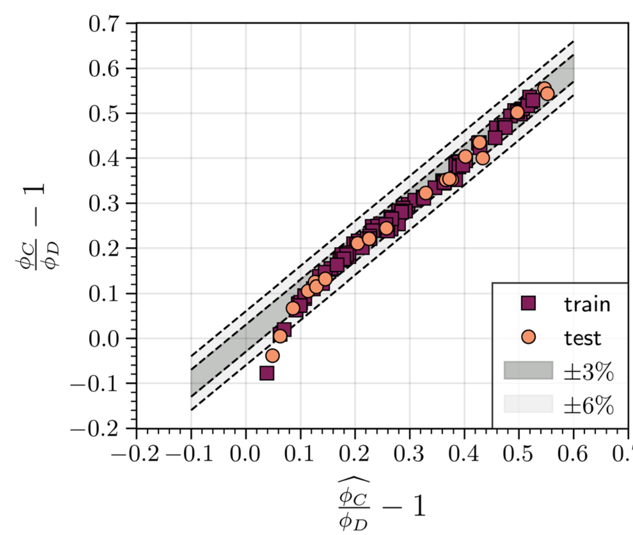

Figure 7: Parity plot between the correlation predictions and the CFD estimates of the choked flow rate.

DOI: 10.17185/duepublico/83307

ASSUMPTION CHECK: INFLUENCE OF THE PERIPHERAL MACH NUMBER

The correlation demonstrates good accuracy, with most predictions falling within the experimental-validation margin of ±3 percentage points, making it a reliable surrogate for Equation (6). However, Equation (6) was derived under two simplifying assumptions: the two-phase flow (characterized by parameter $\mathcal{C}$) and the nature of the two-phase flow (indirectly represented by parameter k) are the primary factors determining the choked flow rate, outweighing the influence of peripheral Mach number variations (although implicitly included in $\mathcal{C}$) and the impeller geometry. To assess the validity of the first assumption, the correlation is tested against variations in the peripheral Mach number.

The same compressor and methodology used during the regression process are also applied here, but considering different peripheral Mach numbers. Four conditions, listed in Table 1, are selected to cover a range of k and $\mathcal{C}$ values, with peripheral Mach numbers varying from 0.5 to 0.9 - typical for compressors in sCO_2 power cycles.

Table 1: Selected cases to check the effect of peripheral Mach number on the choked flow rate.

case	P_0 [bar]	T_0 [K]	k	$\mathcal{C}$	M_u
#1M	81.9	309.20	1.8	1.41	0.72
#2M	93.3	308.30	6.3	0.67	0.89
#3M	71.8	302.18	5.1	0.35	0.50
#4M	103.3	318.06	3.0	1.98	0.81

Figure 8 compares the choked flow rates predicted by the correlation with those obtained via CFD. Significant discrepancies are observed, except for Case #1M, which features a peripheral Mach number of 0.72, close to the value used during regression. In the other cases, deviations reach up to 7.8%. Specifically, for Cases #2M and #4M, which have higher peripheral Mach numbers, the correlation overpredicts the actual choked flow rate. Conversely, in Case #3M, where the peripheral Mach number is lower than the reference, the correlation underpredicts the choked flow rate.

These results indicate that the assumption of implicitly incorporating the peripheral Mach number within $\mathcal{C}$ is inadequate. The effect of the peripheral Mach number extends beyond its contribution to $\mathcal{C}$. While the free-stream Mach number for single-phase flow is generally low, it still modulates two-phase effects, which remain the dominant factor causing choking in all cases. Specifically, as the peripheral Mach number increases, the margin to choking decreases regardless of $\mathcal{C}$, and vice versa.

This analysis underscores the need for future correlations to explicitly account for the influence of the peripheral Mach number, ensuring more accurate predictions across a broader range of operating conditions.

ASSUMPTION CHECK: INFLUENCE OF THE IMPELLER GEOMETRY

In this section, the second assumption regarding the impact of impeller geometry on choking is revised. Specifically, the objective is to determine the extent to which a correlation based on Equation (6) can also represent Equation (5). Achieving complete similitude would require strict geometric similarity; however, given that most impellers for similar applications share comparable designs, it was assumed that variations in geometry have a minor effect compared to changes in thermodynamic conditions, and the two factors do not interact significantly.

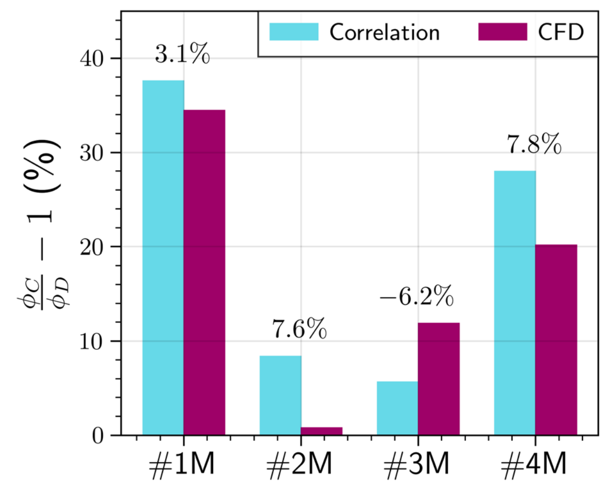

Figure 8: Choked flow estimates obtained through the correlation reported in Equation (7) and CFD simulations. On top of the bars, the difference between the correlation and CFD predictions is reported.

To test this assumption, a second compressor design is considered. The compressor configuration remains a shrouded impeller coupled with a vaneless diffuser, but modifications are made to the impeller, as it is the primary component influencing choking. The new impeller design features a flow coefficient of $\phi_D = 0.06$. The two geometries share the same design work coefficient. The meridional flow paths of the reference and modified impellers are shown in Figure 9. As demonstrated numerically by Romei et al. [14], the choking limit is relatively insensitive to changes in the design flow coefficient, as a larger throat area is counterbalanced by greater flow acceleration.

To further highlight differences in choking behavior, modifications are made to the impeller geometry in line with findings from meridional channel optimization reported in Romei et al. [14]. These include slightly shifting the splitter downstream and, more notably, reducing the curvature of the shroud contours. This adjustment increases the throat area, enhancing the impeller's swallowing capacity. However, as a tradeoff (though not relevant to this study) the surge margin decreases due to increased aerodynamic loading on the impeller.

To isolate the geometric effects, the peripheral Mach number is held constant at 0.70, the same value used in the

DOI: 10.17185/duepublico/83307

regression. Three thermodynamic conditions, spanning different values of k and $\mathcal{C}$, are analyzed as detailed in Table 2.

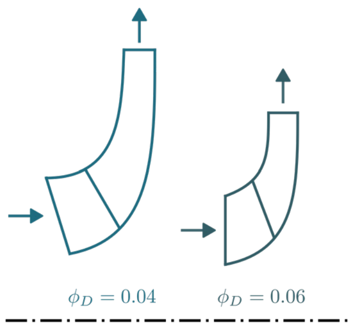

Figure 9: The two different compressor geometry. On the left, the meridional channel of the compressor used for the regression model. On the right, the employed compressor to check the effect of a geometry change.

Table 2: Selected case to check the effect of compressor geometry on the choked flow rate.

case	P_0 [bar]	T_0 [K]	k	$\mathcal{C}$	M_u
#1G	85.0	306.15	5.9	0.59	0.70
#2G	85.0	304.15	7.9	0.53	0.70
#3G	85.0	308.15	4.0	0.71	0.70

Given the high swallowing capacity of the new impeller design, it is expected that the correlation will naturally fail to predict the correct choked flow rate. However, if this discrepancy is purely a geometric offset, as initially assumed, the correlation predictions can be corrected. This can be done by referencing a baseline speedline, determining the ratio between the actual choked flow rate for the reference speedline and the value predicted by the correlation. The corrected choked flow rate for any thermodynamic state can then be computed using the following relationship:

$$\left(\frac{\widehat{\phi_C}}{\phi_D} - 1\right)_{\#i,corr} = \left(\frac{\widehat{\phi_C}}{\phi_D} - 1\right)_{\#i} \cdot \frac{\left(\frac{\phi_C}{\phi_D} - 1\right)_{ref}}{\left(\frac{\widehat{\phi_C}}{\phi_D} - 1\right)_{ref}} \tag{8}$$

The pedices refer to different thermodynamic states, where *ref* denotes the reference speedline of a specific thermodynamic state. For this reference state, the ratio between the actual choking flow rate and the value predicted by the correlation is calculated. This ratio captures the difference in swallowing capacity of the new impeller design compared to the design used in the correlation training. The computed factor is then applied to adjust the correlation's predicted choked flow rate for any generic *i-th* thermodynamic state.

For example, if a new compressor design inherently doubles the choked flow rate for a given thermodynamic condition, the corrective factor will be 2, and this same factor will be applied to adjust the choked flow rate predicted by the correlation under other thermodynamic conditions.

CFD simulations for the three test cases (#1G, #2G, and #3G) yield choked flow rates of $\frac{\widehat{\phi_C}}{\phi_D} - 1$ equal to 18.0%, 10.6%, and 28.6%, respectively, while the correlation predicts values of 7.7%, 6.4%, and 11.2%. From a qualitative perspective, the trends align, but as expected, the absolute values differ significantly due to the new impeller design. The corrected values, calculated using Equation (8), and their deviations from the CFD results are summarized in Table 3, with each of the three cases being treated as the reference for the correction.

Notably, the error in the corrected values depends on the choice of the reference case. In two cases, the error remains below the experimental accuracy threshold of ±3 points, but in the worst-case scenario, it rises to 10 points. This variability is an undesirable feature that challenges the initial assumption of a purely geometric correction factor.

Theoretically, if the offset was purely geometric, the corrective factor should remain constant regardless of the reference case. However, this is not observed, suggesting an interaction between the impeller geometry and local aero-thermodynamic conditions. This finding also underscores that the impact of geometry cannot be fully captured by simple geometric parameters alone, as a simple corrective factor. Instead, it requires consideration of additional aerodynamic factors, such as loading effects, to account for the interplay between geometry and the flow dynamics, which changes as the thermodynamic state varies.

Table 3: Deviation in percentage points between the corrected choked flow rate and the CFD value.

reference	#1G	#2G	#3G
#1G		4.3%	-2.5%
#2G	-5.1%		-10.0%
#3G	1.7%	5.7%	

CONCLUSION

This work aimed to derive a scaling procedure for speed lines of compressors operating with carbon dioxide near the critical point under variable intake thermodynamic conditions. Initially, the deviations from perfect-gas similarity were highlighted, emphasizing the importance of non-ideal gas effects and two-phase flow phenomena. Selective cases were analyzed to illustrate these effects, demonstrating that the primary discrepancies emerge near the choked flow rate.

The choked flow rate was found to be highly sensitive to intake thermodynamic conditions. Consequently, the goal was to establish a correlation linking the choked flow rate to the intake thermodynamic state. This was achieved by parameterizing the conditions with two dimensionless parameters: a generalized cavitation/condensation parameter and the pressure-volume

DOI: 10.17185/duepublico/83307

isentropic coefficient. Together, these parameters describe both the extent and the nature of two-phase effects, distinguishing between cavitation and condensation phenomena.

Using a substantial dataset of CFD simulations, comprising 100 speedlines at a fixed peripheral Mach number but varying thermodynamic states, a symbolic regression algorithm based on gene expression programming was employed. This yielded an analytical relationship to predict the choked flow rate as a function of the two introduced generalized parameters. The underlying assumption was that the variations in these two parameters dominated choking behavior, with other factors, such as the peripheral Mach number and impeller geometry, contributing only with second-order effects.

However, subsequent validation of this assumption revealed its limitations. The results showed that peripheral Mach number and impeller geometry interact with the two-phase non-ideal aero-thermodynamics in unpredictable ways. Therefore, any accurate correlation for predicting the choked flow rate must account for all these factors, including peripheral Mach number, the cavitation/condensation parameter, the pressure-volume isentropic coefficient, geometrical parameters, and loading-related factors.

While the peripheral Mach number can be integrated straightforwardly into an expanded design of experiments, incorporating geometric and loading parameters introduces significant complexity. This complexity undermines the practicality of developing an easy-to-use correlation for scaling performance maps. Furthermore, scaling correlations are most useful in the early design phases, where geometry details and other characteristic parameters are often unavailable.

The interplay of effects near the critical point highlights the inherent challenges of creating a universal scaling correlation. Although the correlation developed in this work is not quantitatively reliable, it provides valuable preliminary insights into trends. For accurate choking evaluations, however, high-fidelity CFD simulations remain essential.

NOMENCLATURE

c	Speed of sound
c_p	Specific heat at constant pressure
c_v	Specific heat at constant volume
$\mathcal{C}$	Cavitation/condensation parameter
f	Radius ratio D_1/D_2
h	Specific enthalpy
h_{sat}	Specific enthalpy at saturation
k	Pressure-volume isentropic coefficient
M_u	peripheral Mach number
P	Pressure
Re_u	Peripheral Reynolds number
s	Specific entropy
T	Temperature
u_1	Peripheral speed at inducer mean radius
u_2	Peripheral speed at impeller outlet
η	Total-total isentropic efficiency
λ	Work coefficient
λ_{eul}	Eulerian work coefficient
μ	Dynamic viscosity
Π	Total-total pressure ratio
ρ	Density
ϕ_2	Outlet flow coefficient
ϕ_D	Design flow coefficient
ϕ_C	Choked-flow coefficient

REFERENCES

[1] M. Casey and C. Robinson, "A method to estimate the performance map of a centrifugal compressor stage," ASME Journal of Turbomachinery, vol. 135, no. 2, p. 021034, 2013.

[2] N. D. Baltadjiev, C. Lettieri, and Z. S. Spakovszky, "An investigation of real gas effects in supercritical CO2 centrifugal compressors," ASME Journal of Turbomachinery, vol. 137, no. 9, p. 091003, 2015.

[3] S. A. Wright, T. M. Conboy, R. F. Radel, and G. E. Rochau, "Modeling and experimental results for condensing supercritical CO2 power cycles," Technical Report, 2011, doi: 10.2172/1030354.

[4] A. J. Glassman, Turbine Design and Application. Washington: NASA Scientific and Technical Information Office, 1971.

[5] H. S. Pham, N. Alpy, J. H. Ferrasse, O. Boutin, M. Tothill, J. Quenaut, O. Gastaldi, T. Cadiou, and M. Saez, "An approach for establishing the performance maps of the sc-CO2 compressor: Development and qualification by means of CFD simulations," International Journal of Heat and Fluid Flow, vol. 61, pt. B, pp. 379–394, 2016.

[6] L. Toni, E. F. Bellobuono, R. Valente, A. Romei, P. Gaetani, and G. Persico, "Computational and experimental assessment of a MW-scale supercritical CO2 compressor operating in multiple near-critical conditions," ASME Journal of Engineering for Gas Turbines and Power, vol. 144, no. 10, p. 101015, Oct. 2022.

[7] J. Mortzheim, D. Hofer, S. Piebe, A. McClung, J. J. Moore, and C. Stefan, "Challenges with measuring supercritical CO2 compressor performance when approaching the liquid-vapor dome," in Proceedings of ASME Turbo Expo 2021, GT2021-59527.

[8] A. Romei, P. Gaetani, and G. Persico, "On sCO2 compressor performance maps at variable intake thermodynamic conditions," in Proceedings of ASME Turbo Expo 2021, vol. 10, V010T30A028.

[9] M. Anderson, "Compressor map corrections for highly non-linear fluid properties," in Proceedings of ASME Turbo Expo 2021, vol. 10, V010T30A029.

[10] A. Romei, P. Gaetani, and G. Persico, "Computational fluid-dynamic investigation of a centrifugal compressor with inlet guide vanes for supercritical carbon dioxide power systems," Energy, vol. 255, 2022.

[11] R. Span and W. Wagner, "A new equation of state for carbon dioxide covering the fluid region from the triple-point temperature to 1100 K at pressures up to 800 MPa," Journal of Physical and Chemical Reference Data, vol. 25, no. 6, pp. 1509–1596, 1996, doi: 10.1063/1.555991.

[12] A. Fenghour, W. Wakeham, and V. Vesovic, "The viscosity of carbon dioxide," Journal of Physical and Chemical Reference Data, vol. 27, no. 1, pp. 31–39, 1998, doi: 10.1063/1.556013.

[13] G. Scalabrin, P. Marchi, F. Finezzo, and R. Span, "A reference multiparameter thermal conductivity equation for carbon dioxide with an optimized functional form," Journal of Physical and Chemical Reference Data, vol. 35, no. 4, pp. 1549–1575, 2006, doi: 10.1063/1.2213631.

[14] A. Romei, P. Gaetani, and G. Persico, "Guidelines for the aerodynamic design of sCO2 centrifugal compressor stages," ASME

DOI: 10.17185/duepublico/83307

Journal of Engineering for Gas Turbines and Power, vol. 145, no. 11, p. 111014, Nov. 2023.

[15] G. Persico, A. Romei, P. Gaetani, E. F. Bellobuono, L. Toni, and R. Valente, "Thermo-fluid dynamic modeling of a supercritical carbon dioxide compressor for waste heat recovery applications," Energy, vol. 294, p. 130874, 2024.

[16] M. Casey and C. Robinson, Radial Flow Turbocompressors: Design, Analysis, and Applications. Cambridge: Cambridge University Press, 2021, doi: 10.1017/9781108241663.

[17] M. Masi, L. Da Lio, and A. Lazzaretto, "An insight into the similarity approach to predict the maximum efficiency of organic Rankine cycle turbines," Energy, vol. 198, p. 117278, 2020.

[18] D. Baumgärtner, J. J. Otter, and A. P. S. Wheeler, "The effect of isentropic exponent on transonic turbine performance," ASME Journal of Turbomachinery, vol. 142, no. 8, p. 081007, Aug. 2020.

 DOI: 10.17185/duepublico/83307

DOI: 10.17185/duepublico/83307
URN: urn:nbn:de:hbz:465-20250428-102136-0